Sains Malaysiana 55(5)(2026): 898-914
http://doi.org/10.17576/jsm-2026-5505-12

Synthesis, *In Silico* Study, and *In Vitro* Essay of Pyridazinone-Hydrazone Hybrid as Inhibitor for α-Glucosidase

(Sintesis, Kajian *In silico* dan Esei *In Vitro* Hibrid Piridazinon-Hidrazon sebagai Perencat α-Glukosidase)

YUNI FATISA[1,2], HENLI HENLI[1], NENI FRIMAYANTI[3], HILWAN YUDA TERUNA[1] & JASRIL JASRIL[1,*]

[1]*Department of Chemistry, Faculty of Mathematics and Natural Sciences, Universitas Riau, Pekanbaru (28293), Indonesia*
[2]*Department of Chemistry Education, Faculty of Tarbiyah and Keguruan, Universitas Islam Negeri Sultan Syarif Kasim Riau, Pekanbaru (28293), Indonesia*
[3]*Department of Pharmacy, Sekolah Tinggi Ilmu Farmasi Riau, Pekanbaru (28293), Indonesia*

Received: 16 October 2025/Accepted: 28 April 2026

ABSTRACT

Although pyridazinone derivatives as α-glucosidase inhibitors have been reported as potential α-glucosidase inhibitors, studies in this area remains limited, and require further studies exploration. Current α-glucosidase inhibitor therapies, such as acarbose, are effective but may cause undesirable side effects in some patients. This study aimed to synthesise new pyridazinone-hydrazone hybrids (**7a–f**) and evaluate their potential as α-glucosidase inhibitors targeting the 3A4A receptor. The compounds were synthesized by reacting compound **5** with various hydrazines via a microwave-assisted addition-elimination reaction. Structural characterizations were performed using FTIR, HRMS, ^{1}H-NMR, and ^{13}C-NMR spectroscopy. Antidiabetic activity was investigated using molecular docking with MOE 2024, density functional theory (DFT) calculations with GaussView 5.0, *in vitro* α-glucosidase inhibition assays, and ADMET predictions using the pkCSM and ProTo-x-II servers. Microwave irradiation enabled the efficient synthesis of the target compounds (**7a-f**) in good yields with significantly reduced reaction times (3-10 min). Molecular docking predicted favorable binding free energies comparable to acarbose and indicated stable non-covalent interactions with key residues in the enzyme active site. DFT analysis showed favorable electronic properties with small HOMO-LUMO energy gaps for the synthesized complexes. *In vitro* assays confirmed that compounds **7a–c** exhibited strong inhibitory activity, with IC_{50} values of 26.33, 18.80, and 12.35 μg/mL, respectively, although acarbose remained more potent (IC_{50} = 0.01 μg/mL). ADMET predictions indicated potential limitations in terms of oral bioavailability. These findings highlight pyridazinone–hydrazone hybrids as promising α-glucosidase inhibitors and suggest that further structure–activity relationship (SAR) optimization is required to improve their pharmacokinetic properties.

Keywords: ADMET; DFT; molecular docking; pyridazinone; α-glucosidase enzyme

ABSTRAK

Walaupun kajian berkaitan potensi terbitan piridazinone sebagai perencat α-glukosidase telah dilaporkan, tetapi penyelidikannya masih terhad dan keputusan yang diperoleh memerlukan penambahbaikan selanjutnya. Terapi perencat α-glukosidase seperti akarbose telah terbukti berkesan tetapi mempunyai kesan sampingan. Objektif penyelidikan ini adalah untuk mensintesis hibrid piridazinone-hidrazon (**7a-f**), menganalisis keberkesanannya merencat aktiviti α-glukosidase (3A4A). Sintesis sebatian **7a-f** dijalankan melalui tindak balas antara sebatian **5** dan pelbagai kumpulan hidrazin menggunakan penyinaran gelombang mikro melalui tindak balas penambahan-penyingkiran. Pencirian produk menggunakan spektroskopi FTIR, HRMS, ^{1}H-NMR dan ^{13}C-NMR. Aktiviti α-glukosidase (3A4A) dinilai melalui pendokan molekul menggunakan perisian MOE 2024.0901 dan DFT menggunakan perisian Gaussian view 5.0, ujian *in vitro* profil α-glukosidase dan meramalkan profil ADMET menggunakan pKCSm dan ProTox II. Kaedah penyinaran gelombang mikro membolehkan sintesis sebatian (**7a-f**) memberikan hasil yang baik dengan masa tindak balas yang cepat (3-10 min). Pendokan molekul menunjukkan sebatian **7a-f** mempunyai nilai tenaga bebas pengikat hampir sama dengan akarbose, membentuk interaksi bukan kovalen dan membentuk sentuhan dengan residu pada tapak aktif reseptor. Analisis DFT menunjukkan sifat elektronik yang baik dan tenaga HOMO-LUMO GAP yang kecil. Ujian *in vitro* menunjukkan bahawa akarbose adalah perencat yang sangat aktif (IC_{50} 0.01 μg/mL), manakala sebatian **7a-c** aktif sebagai perencat α-glukosidase dengan nilai IC_{50} 26.33, 18.80 dan 12.35 μg/mL. Kajian farmakokinetik memberikan cabaran utama untuk bioketersediaan oral. Analisis struktur-aktiviti hubungan (SAR) diperlukan untuk mereka bentuk sebatian terbitan baharu daripada hibrid piridazinon-hidrazon ini yang boleh mengekalkan potensi perencatan yang berkesan tetapi dengan sifat farmakokinetik yang lebih baik.

Kata kunci: ADMET; DFT; enzim α-glukosidase; pendokan molekul; piridazinon

INTRODUCTION

The pyridazinone ring is an attractive scaffold because the nitrogen atom, carbonyl group, and functionalisation at various positions on the pyridazinone ring can be designed as active moieties for the discovery of many new pyridazinone derivatives. γ-Keto acids, which are precursors in pyridazinone synthesis, can be substituted with specific functional groups to diversify pyridazinone structures.

One increasingly popular method is the design and synthesis of hybrid compounds, which exploits the synergistic effects of combined pharmacophores to produce molecules with low side effects and high biological activity. This strategy expands the opportunities for discovering novel pyridazinone derivatives with various biological activities, such as antioxidant (Khokra et al. 2016), COX-2 inhibitor (Abida et al. 2020; Ahmed et al. 2019), antimicrobial (Nagle et al. 2014), and BuChE selective inhibitor (Dundar et al. 2019), aldose reductase inhibitor (Akdağ et al. 2022; Yaseen et al. 2016), DPP-4 inhibitors and antihyperglycaemic (Nidhar et al. 2023), and an α-glucosidase enzyme inhibitor (Assila et al. 2024; Chaudhry et al. 2017; Firoozpour et al. 2023; Moghimi et al. 2020). Recent studies have demonstrated the antidiabetic potential of various hydrazone derivatives (Altıntop et al. 2023; Hafiza Zara et al. 2023; Shayegan et al. 2023). Previous studies have extensively reported the synthesis of various hydrazone-pyridazinone derivatives, demonstrating their excellent bioactive agents as cyclooxygenase-2 inhibitors (Abida et al. 2020).

Type 2 diabetes mellitus (T2DM) accounts for approximately 90% of all types of diabetes. Diabetes is a dangerous disease because poor blood sugar management over a long period of time can lead to complications such as cardiovascular disease, stroke, coronary heart disease, retinopathy, cataracts, and kidney failure, as well as a decline in quality of life and life expectancy (Abuelizz et al. 2019; Keri et al. 2015). One mechanism of T2DM diabetes treatment is α-glucosidase enzyme inhibitors (AGIs). AGIs inhibit the activity of the α-glucosidase enzyme to hydrolyse polysaccharides into glucose in the small intestine wall, thereby slowing glucose absorption and preventing an increase in blood glucose levels (Lebovitz 1997). Treatment with α-glucosidase enzyme inhibitors is primarily used in patients with postprandial hyperglycaemia and prediabetes. This therapy is preferred because it does not cause hypoglycaemia, can be used as monotherapy, and is safe to combine with other antidiabetic drugs for synergistic effects (Hedrington & Davis 2019; Pakkir Maideen 2019).

Extensive research has been conducted on antidiabetic discoveries. Currently, only three α-glucosidase inhibitors are used clinically, namely acarbose, voglibose, and miglitol. Acarbose is the most commonly prescribed α-glucosidase enzyme inhibitor. While acarbose is metabolised by gut bacteria and digestive enzymes, its fermentation of unabsorbed carbohydrates can increase colonic gas, leading to side effects such as diarrhoea, flatulence, and meteorism. Therefore, treatment with acarbose must be used very carefully, especially in patients with hypersensitivity to the drug, inflammatory bowel disease, colonic ulceration, or partial intestinal obstruction (Derosa & Maffioli 2012). Despite having milder side effects, miglitol and voglibose are less effective in inhibiting α-glucosidase enzyme activity compared to acarbose. Based on these, it is obvious that the available α-glucosidase enzyme inhibitor agents are still limited and have various side effects. This trade-off between efficacy and safety underscores the necessity for novel antidiabetic medicines that are both effective and well-tolerated. Regarding pyridazinone derivatives, there have been many relevant studies, as mentioned earlier, where they have antidiabetic activity, but none of these pyridazinone derivatives have reached registered medicine status.

Encouraged by these findings, and in continuation of our interest in developing novel pyridazinone derivatives, we hypothesised that combining both the hydrazone and pyridazinone scaffolds into a single molecular framework could lead to new hybrids. To the best of our knowledge, there are no reports on the synthesis of compounds combining these specific pharmacophores based on our approach. Therefore, the synthesis of novel pyridazinone-hydrazone hybrid structures is of considerable interest for expanding the chemical space of bioactive molecules as more promising and safer alternative candidates for antidiabetic agents. The synthesis was carried out in several reaction stages. The initial stage was an aldol condensation mechanism between 4-methoxyacetophenone, glyoxylic acid, and hydrazine, producing compound **3**. In the second stage, compound **5** was synthesised as a linker molecule via an aromatic nucleophilic substitution (SNAr) reaction between compound **3** and 4-fluoroacetophenone. In the third stage, compound **5** is reacted with various hydrazide derivatives to produce the target compounds, which are new pyridazinone hydrazone derivatives (**7a-f**).

The activity of target compounds as α-glucosidase enzyme inhibitors was evaluated *in silico* using molecular docking and density functional theory (DFT) approaches and *in vitro* α-glucosidase enzyme inhibition assays. This approach aims to facilitate preliminary information regarding the bioactivity of drug candidates. The molecular docking method used the Molecular Operating Environment (MOE) 2024.0901 software to predict binding free energy value and the type of ligand-protein complex interaction. DFT analysis was performed using Gaussian View 5.0 software to calculate the energy levels of molecular structures in various electronic configurations of target compounds using quantum mechanics. Furthermore, the pharmacokinetic profile of target compounds will be predicted.

MATERIALS AND METHODS

All reagents were used without further purification: 4-methoxy acetophenone (Sigma-Aldrich), hydrazine

(Sigma-Aldrich), glyoxylic acid (Sigma-Aldrich), 4-fluoro acetophenone (Sigma-Aldrich), glacial acetic acid (Merck), 4-methylbenzenesulfonhydrazide (Merck), potassium carbonate (Merck), p-nitrophenyl-α-D-glucopyranoside, and organic solvents. The synthesis reaction was carried out using a sealed-vessel reactor, Monowave 50 (Anton-Paar, Graz, Austria). The melting point was determined on a Fisher-Johns apparatus (Fisher Scientific, Waltham, MA, USA) (uncorrected). HPLC (UFLC Prominence Shimadzu LC Solution, detector UV SPD 20AD). The HPLC system was equipped with a Shim-pack VP-ODS column (250 mm × 4.6 mm). The mobile phase consisted of acetonitrile and water, delivered at a flow rate of 0.75 mL/min under gradient elution conditions. All samples were filtered through a 0.45 µm PTFE syringe filter (Grace) prior to analysis. Thin layer chromatography (TLC) analysis was carried out using GF254 (Merck Millipore, Darmstadt, Germany) under a UV lamp 254/365 nm (Cole-Elmer®, Vernon Hills, IL, USA). The FT-IR spectrum was recorded in KBr powder on a Shimadzu® FT-IR Prestige-21 spectrophotometer (Shimadzu Corporation, Kyoto, Japan), and the mass spectrum was measured using a Waters Xevo QTOFMS instrument (Waters, Milford, MA, USA). The ^{1}H-NMR and ^{13}C-NMR spectra were recorded on an Agilent® (Agilent Technologies, Santa Clara, CA, USA) at 500 MHz and 125 MHz, respectively. The molecular docking was carried out using the MOE 2024.0901 software package and Discovery Studio Visualizer (DSV) 2019 software.

The research synthesis was carried out in three stages: the first stage was an aldol condensation (the Claisen-Schmidt reaction) performed via the one-pot method (Cruz et al. 2016; Yuni et al. 2025); the second stage was a monowave-assisted SNAr reaction (Abida et al. 2020); and the third stage was a microwave-assisted reaction (Can et al. 2017). Molecular docking was performed using MOE 2024.0901 software, while DFT calculations were conducted in Gaussian View 5.0 (Frimayanti et al. 2025). Pharmacokinetic (ADME) and toxicity predictions were carried out using the pkCSM and ProTox-II web servers. The alpha-glucosidase enzyme inhibition assay was used to evaluate the *in vitro* antidiabetic efficacy (Liu et al. 2020; Teni et al. 2017).

SYNTHESIS OF COMPOUNDS **7A-F**

Synthesis of [6-(4-methoxyphenyl-pyridazin-3(2H)-one] (3): The synthesis of compound **3** was carried out by modifying the procedure proposed by Cruz et al. (2016) and Yuni et al. (2025).

Synthesis of [2-(4-acetylphenyl)-6-(4-methoxyphenyl) pyridazin-3(2H)-one] (5): The synthesis of compound **5** was carried out by modifying the procedure proposed by Abida et al. (2020). A mixture of 1 mmol of compound **3**, 1.25 mmol of 4-fluoroacetophenone (**4**), and 1 mmol of potassium carbonate in 4 mL of DMF was reacted at 100 °C for 16 h using a Monowave 50 heater. Reaction control was performed using TLC with a mixture of n-hexane and ethyl acetate (6:4) as the eluent. The reaction mixture was poured into ice water (10 mL). The precipitate was filtered and washed with cold demineralised (DM) water (25 mL), then dried at room temperature. After that, the precipitate of **5** was recrystallised with hot n-ethanol (10 mL) and then dried at room temperature. Next, the solid obtained was tested for purity using TLC, melting point measurement, and HPLC analysis. Structural elucidation was performed using FT-IR, HRMS, and ^{1}H-NMR.

*Compound **(5)*** The molecular formula $C_{19}H_{16}N_2O_3$; light brown solid; yield 23.06 %; M.p: 152-154 °C; Rf = 0,30 (n-hexana : ethyl acetate = 6 : 4); HPLC chromatogram: tR = 5.08 min (254 nm) and tR = 5.08 min (365 nm); UV spectrum (EtOH) Abs: 0.478 (λ_{max} 258 nm), 0.139 (λ_{max} 346 nm); FT-IR spectrum (KBr) $\bar{U}$ (cm^{-1}): 3069 (aromatic C-H), 2959 (sp^3 aliphatic C-H), 1676 (ketone C=O), 1518 (C=N), 1363 (C-N), 1032 (C-O); ^{1}H-NMR spectrum (500 MHz, $CDCl_3$), δ (ppm): 8.10 (d, *J* = 8.7 Hz, 2H), 7.91 (d, *J* = 8.7 Hz, 2H), 7.79 (d, *J* = 8.9 Hz, 2H), 7.75 (d, *J* = 9.8 Hz, 1H), 7.14 (d, *J* = 9.8 Hz, 1H), 7.00 (d, *J* = 8.9 Hz, 2H), 3.88 (s, 3H), 2.66 (s, 3H); The HRMS spectrum (m/z) calculated: $C_{19}H_{16}N_2O_3$ $[M+H]^+$: 321.1239, found: (m/z) $[M+H]^+$: 321.1246.

*Synthesis of **7a-f**:* The synthesis of compounds **7a-f** was carried out by modifying the procedure proposed by Can et al. (2017). A mixture of 1 mmol of compound **5** and 4 mmol of hydrazide derivatives (**6a-d**) was placed in a reactor tube, then 5 mL of absolute ethanol and 3 mL of glacial acetic acid were added. The mixture was then irradiated using a microwave device at medium-low power for 3-10 min. Reaction control was performed every 1 min using TLC with hexane:ethyl acetate (4:6) as the eluent. After that, the pH of the mixture was neutralised (pH 7) with 10 mL of 6 N NaOH solution. The precipitate was filtered and washed with cold demineralised (DM) water (25 mL) and cold n-hexane, then dried at room temperature. The impure sample solid was recrystallised. The purity of the solid obtained was tested using TLC, melting point and HPLC analysis. Structural elucidation was performed using FTIR, HRMS, ^{1}H-NMR, and ^{13}C-NMR.

*Compound [(E)-N'-(1-(4-(3-(4-methoxyphenyl)-6-oxopyridazin-1(6H)-yl)phenyl)ethylidene) benzohydrazide] **(7a)**:* Molecular formula $C_{26}H_{22}N_4O_3$; brownish-yellow solid; yield 77.50 %; Rf = 0,40 (n-hexana : ethyl acetate = 4 : 6); M.p 179-180 °C; HPLC chromatogram tR = 7.88 min (296 nm) and tR = 7.88 min (365 nm); UV spectrum (EtOH) Abs: 0.602 (λ max 277 nm), 0.203 (λ max 340 nm); FT-IR spectrum (KBr) $\bar{U}$ (cm^{-1}): 3247 (NH), 3054 (aromatic C-H), 2968 (sp^3 aliphatic C-H), 1673 (ketone C=O), 1515 (C=N), 1256 (C-N), 1175 (C-O); ^{1}H-NMR (500 MHz, $CDCl_3$) δ 9.34 (s, 1H), 7.97 (s, 2H), 7.89 (s, 2H), 7.75 (dd, *J* = 14.4; 8.3 Hz, 4H), 7.69

(d, *J* = 9.6 Hz, 1H), 7.54 (t, *J* = 7.4 Hz, 1H), 7.47 (t, *J* = 7.5 Hz, 2H), 7.05 (s, 1H), 6.98 (d, *J* = 8.4 Hz, 2H), 3.86 (s, 3H), 2.32 (s, 3H); ^{13}C-NMR spectrum (126 MHz, $CDCl_3$), δ (ppm): 161.0; 159.4; 144.9; 137.3; 131.8; 131.2; 130.2; 128.8; 127.5; 127.1; 126.9; 126.6; 125.2; 114.4; 55.4; 18.4. The HRMS spectrum (m/z) calculated: $C_{26}H_{22}N_4O_3$ $[M+H]^+$: 439.1764, found: (m/z) $[M+H]^+$: 439.1770.

Compound [(E)-2-(1-(4-(3-(4-methoxyphenyl)-6-oxopyridazin-1(6H)-yl)phenyl)ethylidene)-N-phenylhydrazine-1-carbothioamide] ***(7b)****:* Molecular formula $C_{26}H_{23}N_5O_2S$; yellow solid; yield 59.90 %; Rf = 0,50 (n-hexsana : ethyl acetate = 4 : 6); M.p 191-192 °C; HPLC chromatogram tR = 9.14 min (254 nm) and tR = 9.14 min (365 nm); UV spectrum (EtOH) Abs: 0.478 (λmax 277 nm); FT-IR spectrum (KBr) Ū (cm^{-1}): 3292 (NH), 3074 (aromatic C-H), 2957 (sp^3 aliphatic C-H), 1671 (ketone C=O), 1550 (C=N), 1256 (C-N), 1186 (C-O); ^{1}H-NMR spectrum (500 MHz, $CDCl_3$), δ (ppm): δ 9.43 (s, 1H), 8.86 (s, 1H), 7.86 (q, *J* = 8.9 Hz, 4H), 7.79 (d, *J* = 8.9 Hz, 2H), 7.75 (d, *J* = 9.9 Hz, 1H), 7.71 (d, *J* = 7.4 Hz, 2H), 7.43 (t, *J* = 8.0 Hz, 2H), 7.27 (s, 1H), 7.15 (d, *J* = 9.8 Hz, 1H), 7.00 (d, *J* = 8.9 Hz, 2H), 3.88 (s, 3H), 2.39 (s, 3H); ^{13}C-NMR spectrum (126 MHz, $CDCl_3$), δ (ppm): 176.3; 161.0; 159.4; 146.2; 145.0; 143.0; 137.8; 136.7; 131.5; 130.2; 128.8; 127.5; 126.8; 126.8; 126.2; 125.5; 124.2; 114.4; 55.4; 13.8; The HRMS spectrum (m/z) calculated: $C_{26}H_{23}N_5O_2S$ $[M+H]^+$: 470.1651, found: (m/z) $[M+H]^+$: 470.1635.

Compound [(E)-N'-(1-(4-(3-(4-methoxyphenyl)-6-oxopyridazin-1(6H)-yl)phenyl)ethylidene)-4-methylbenzenesulfonohydrazide] ***(7c)****:* Molecular formula $C_{26}H_{24}N_4O_4S$; light yellow solid; yield 16.40 %; Rf = 0,55 (n-hexsana : ethyl acetate = 4 : 6); M.p 168-170 °C; HPLC chromatogram tR = 8.11 (254 nm); 8.11 (365 nm); UV spectrum (EtOH) Abs: 0.505 (λmax 270 nm), 0.1311 (λmax 350 nm); FT-IR spectrum (KBr) Ū (cm^{-1}): 3349 (N-H), 3023 (aromatic C-H), 2912 (sp3 aliphatic C-H), 1667 (ketone C=O), 1599 (C=N), 1334 (C-N), 1159 (C-O), 1276 (SO_2); ^{1}H-NMR spectrum (500 MHz, $CDCl_3$), δ (ppm): 8.09 (s, 1H), 7.92 (d, *J* = 8.0 Hz, 2H), 7.77 (dd, *J* = 13.2; 9.3 Hz, 3H), 7.70 (d, *J* = 8.4 Hz, 2H), 7.62 (d, *J* = 8.3 Hz, 2H), 7.32 (d, *J* = 8.0 Hz, 2H), 7.16 (d, *J* = 9.7 Hz, 1H), 7.00 (d, *J* = 8.9 Hz, 2H), 3.88 (s, 3H), 2.42 (s, 3H), 2.08 (s, 3H); ^{13}C-NMR spectrum (126 MHz, $CDCl_3$), δ (ppm): 161.0; 159.4; 151.4; 145.0; 144.2; 142.6; 136.8; 135.4; 131.4; 130.2; 129.6; 128.5; 128.1; 127.5; 126.6; 125.2; 114.4; 55.4; 21.6; 13.3; HRMS spectrum (m/z) calculated $C_{26}H_{24}N_4O_4S$ $[M+H]^+$: 488.1415, found: (m/z) $[M+H]^+$: 488.1416.

Compound [(E)-N'-(1-(4-(3-(3-methoxyphenyl)-6-oxopyridazin-1(6H)-yl)phenyl)ethylidene) benzohydrazide] ***(7d)****:* Molecular formula $C_{26}H_{22}N_4O_3$; reddish-orange solid; yield 74.40 %; Rf = 0,35 (n-hexana : ethyl acetate = 5 : 5); M.p 168-170 °C; HPLC chromatogram tR = 7.1 (206 nm); 7.1 (254 nm); UV spectrum (EtOH) Abs: 0.592 (λmax 253 nm), 0.608 (λmax 221 nm); FT-IR spectrum (KBr) Ū (cm^{-1}): 3169 (N-H), 3057 (aromatic C-H), 2836 (sp^3 aliphatic C-H), 1653 (amida C=O), 1581 (C=N), 1230 (C-N), 1031 (C-O); ^{1}H-NMR spectrum (500 MHz, $CDCl_3$), δ (ppm): 10.8 (s, 1H, NH), 8.16 (d, *J* = 9,8 Hz, H-5), 8.0 (s, 2H), 7.88 (t, 2H), 7.77 (s, 2H), 7.58 (s, 1H), 7.54-7.49 (m, 3H), 7.45 (s, 1H), 7.42 (t, *J* = 8 Hz), 7.19 (d, *J* = 9,8 Hz, 1H), 7.05 (dd, 1H, *J* = 2,5 Hz, dan *J* = 8 Hz), 3.81 (s, 3H), 2.42 (s, 3H); ^{13}C-NMR spectrum (126 MHz, $CDCl_3$), δ (ppm): 160.1, 159.1, 154.8, 144.6, 142.8, 138.0, 136.0, 134.4, 131.7, 131.5, 130.6, 128.9, 128.8, 128.4, 127.8, 127.1, 125.8, 118.8, 115.7, 111.9, 55.7, 15.0; HRMS spectrum (m/z) calculated $C_{26}H_{22}N_4O_3$ $[M+H]^+$: 439.1770, found: (m/z) $[M+H]^+$: 439.1766.

Compound [(E)-2-(1-(4-(3-(3-methoxyphenyl)-6-oxopyridazin-1(6H)-yl)phenyl)ethylidene)-N-phenylhydrazine-1-carbothioamide] ***(7e)****:* Molecular formula $C_{26}H_{23}N_5O_2S$; light brown; yield 79,20 %; Rf = 0,50 (n-hexana : ethyl acetate = 4 : 6); M.p 142-144 °C; HPLC chromatogram tR = 4.0 min (220 nm) and tR = 4.0 min (314 nm); UV spectrum (EtOH) Abs: 0.271 (λmax 250 nm), 0.233 (λmax 314 nm); FT-IR spectrum (KBr) Ū (cm^{-1}): 3207 (NH), 3049 (aromatic C-H), 2834 (sp^3 aliphatic C-H), 1666 (amida C=O), 1486 (C=N), 1290 (C-N), 1185 (C=S), 1029 (C-O); ^{1}H-NMR spectrum (500 MHz, $CDCl_3$), δ (ppm): 9.43 (s, 1H, NH), 8.89 (s, 1H, NH), 7.88 (d, *J* = 8.8 Hz, 2H), 7.84 (d, *J* = 8.8 Hz, 2H), 7.77 (d, *J* = 9.8 Hz, 1H), 7.71 (d, *J* = 8,0 Hz, 2H), 7.44-7.40 (m, 5H), 7.27 (d, *J* = 7.6 Hz, 1H), 7.16 (d, *J* = 9.8 Hz, 1H), 7.02-6.99 (m, 1H), 3.87 (s, 3H), 2.38 (s, 3H); ^{13}C-NMR spectrum (126 MHz, $CDCl_3$), δ (ppm): 176.3, 160.2 , 159.5, 146.2, 145.0, 142.8, 137.8, 136.9, 135.7, 131.5, 130.5, 130.1, 128.8, 126.8, 126.2 (C-4), 125.5, 124.2, 118.5, 115.2, 111.8, 55.4, 13.8; The HRMS spectrum (m/z) calculated: $C_{26}H_{23}N_5O_2S$ $[M+H]^+$: 470.1651, found: (m/z) $[M+H]^+$: 470.1656.

Compound [(E)-N'-(1-(4-(3-(3-methoxyphenyl)-6-oxopyridazin-1(6H)-yl)phenyl)ethylidene)-4-methylbenzenesulfonohydrazide] ***(7f)****:* Molecular formula $C_{26}H_{24}N_4O_4S$; light yellow solid; yield 50.30 %; Rf = 0,30 (n-hexana : ethyl acetate = 6 : 4); M.p 182-184 °C; HPLC chromatogram tR = 3.8 (257 nm); 3.8 (347 nm); UV spectrum (EtOH) Abs: 0.522 (λmax 257 nm), 0.151 (λmax 347 nm); FT-IR spectrum (KBr) Ū (cm^{-1}): 3105 (N-H), 2842 (aromatic C-H), 1658 (amida C=O), 1593 (C=N), 1289 (C-N), 1035 (C-O), 1169 (SO_2); ^{1}H-NMR spectrum (500 MHz, $CDCl_3$), δ (ppm): 8.05 (s, 1H, NH), 7.90 (d, *J* = 8.0 Hz, 2H), 7.76 (d, *J* = 9.7 Hz, 1H); 7.70 (d, *J* = 8.4 Hz, 2H), 7.61 (d, *J* = 8.4 Hz, 2H), 7.41-7.37 (m, H), 7.31 (d, *J* = 7.9 Hz), 7.16 (d, *J* = 9.7 Hz, 1H), 6.99 (td, *J* = 7.3 and 2.3 Hz, 1H), 3.86 (s, 3H), 2.41 (s, 3H), 2.08 (s, 3H); ^{13}C-NMR spectrum (126 MHz, $CDCl_3$), δ (ppm): 144.9, 151.5, 151.4, 144.9, 144.3, 142.5. 159.5, 135.8, 135.5, 131.5, 130.6, 130.2, 129.7, 128.1, 126.7, 125.3, 118.6, 115.4, 111.8, 55.5, 21.7, 13.4; HRMS spectrum (m/z) calculated $C_{26}H_{24}N_4O_4S$ $[M+H]^+$: 489.1596, found: (m/z) $[M+H]^+$: 489.1604.

MOLECULAR DOCKING

The macromolecule structure of the enzyme α-glucosidase or oligo-1,6-glucosidase was downloaded from the RCSB Protein Data Bank (https://www.rcsb.org/), namely isomaltase from *Saccharomyces cerevisiae* (PDB ID **3A4A**) with a resolution of 1.60 Å, bound to the competitive inhibitor maltose. Receptor preparation was carried out in two stages. In the first stage, the receptor was prepared using DSV to remove water molecules and select native ligands. In the second stage, preparation was continued using MOE to undergo the energy minimisation process, force field determination (CHARMM27), RMS gradient (0.01 kcal/mol/A^2), hydrogen atom addition, x, y, z coordinate value setting, and structure refinement (charge addition, protonation, and missing atom refinement).

Ligand preparation began with each ligand structure drawn using ChemOffice v.17 software. The structures were copied to the MOE interface to undergo the preparation process, which included energy and molecular structure geometry optimisation, selecting the force field (MMF94x), the RMS gradient (0.0001 kcal/mol/A^2), and adding hydrogen atoms and partial charges.

Molecular docking was executed via the Compute menu in MOE. In the docking configuration, the receptor was designated as MOE, the binding site was indicated with a dummy atom, and the ligand database was established as an MDB file. The scoring mechanism was configured to London dG for both initial scoring and rescoring, utilizing a triangle matcher for placement and a rigid receptor for refining. Fifty positions were produced, and the ten most optimal poses were selected. The ultimate conformation was chosen based on the minimal binding free energy and an RMSD value of less than 2 Å. The docking procedure was deemed valid when the RMSD of the native ligand redocking was ≤ 2. Å.

DENSITY FUNCTIONAL THEORY (DFT) STUDY

For the DFT study, ligands with the best conformations from the docking process were selected. DFT was performed according to Abbaz, Bendjeddou and Villemin (2018) and Frimayanti et al. (2025). Each ligand was opened in BIOVIA DSV software and saved in the SybylMol2 format. Next, quantum chemical calculations of the ligands were performed in Gaussian View 5.0 software using the B3LYP model on the 6-31G (d,p) basis set. The 6-31G (d,p) basis set can represent electron orbitals with polarisation functions. The notation (d,p) indicates that the d-type polarisation function (*d* orbitals) is added to all non-hydrogen atoms (C, O, and N atoms), and the p-type polarisation function is added to all hydrogen atoms.

MOLECULAR ELECTROSTATIC POTENTIAL (MEP)

The molecular electrostatic potential (MEP) map is visualised using the GaussView 5.0 application based on the results of the B3LYP/6-31G(d,p) basis set calculation method. The different 3D colour maps on the resulting molecular surface can identify areas with different electron densities (electron donors and electron acceptors), thereby predicting the reactive properties of molecules and intermolecular interactions.

GLUCOSIDASE INHIBITORY ASSAY

The test was performed following the protocol of Liu et al. (2020) and Teni et al. (2017). In a 96-well microplate reader, 10 µL of a 100 µg/mL sample was added with 50 µL of phosphate buffer (pH 7), 25 µL of 20 mM p-NPG, 25 µL of α-glucosidase (0.2 U/mL), then incubated for 30 min at 37 °C. After 30 min, the reaction was stopped by adding 100 µL of 0.1 M Na_2CO_3 solution, and then the absorbance of p-NPG was measured at a wavelength of 410 nm with a UV-VIS spectrophotometer. Testing on a concentration series of 6.25, 12.5, 25, and 50 for samples and acarbose (as a positive control) was carried out using the same method. Meanwhile, 10 µL of DMSO was added to the blank control. Enzymatic inhibitory activity = $(1-Ax/A0) \times 100\%$ (A0 is the OD value of the DMSO blank control and Ax is the test sample. The IC_{50} (inhibitory concentration) value was used as a parameter for α-glucosidase enzyme inhibition. The IC_{50} value is the concentration of the α-glucosidase sample/inhibitor capable of inhibiting 50% of the activity of α-glucosidase under test conditions.

ADMET PROFILES

ADMET predictions were performed online using pKCSM (https://biosig.lab.uq.edu.au/pkcsm/prediction). Ligands in the SMILE format were pasted into the column provided in the SMILES string. Next, the ADMET prediction mode was selected. The results were downloaded and analysed. The drug-likeness profile and toxicity prediction were performed using online ProTox II (https://tox-new.charite.de/protox_II/index.php?site=compound_input). Oral toxicity prediction was based on the LD_{50} dose (mg/kg) (Drwal et al. 2014).

RESULTS AND DISCUSSION

CHEMISTRY

The synthesis of new pyridazinone derivatives, namely new pyridazinone-hydrazone hybrids (**7a-f**), was carried out in three reaction stages (Figure 1).

In the first stage, a mixture of 4-methoxyacetophenone, glyoxylic acid, hydrazine hydrate, and acetic acid as a catalyst undergoes an aldol condensation (the Claisen-Schmidt reaction) in a Monowave 50 reactor. In this study, the one-pot method employed refers to a sequential (cascade) reaction approach (Abdolrahimi et al. 2025). Several reaction steps were carried out consecutively within the same monowave reactor vessel. Firstly, the addition of glyoxylic acid and a substituted acetophenone in the presence of a carboxylic acid catalyst yielded a crotonic acid intermediate, followed by the addition of hydrazine

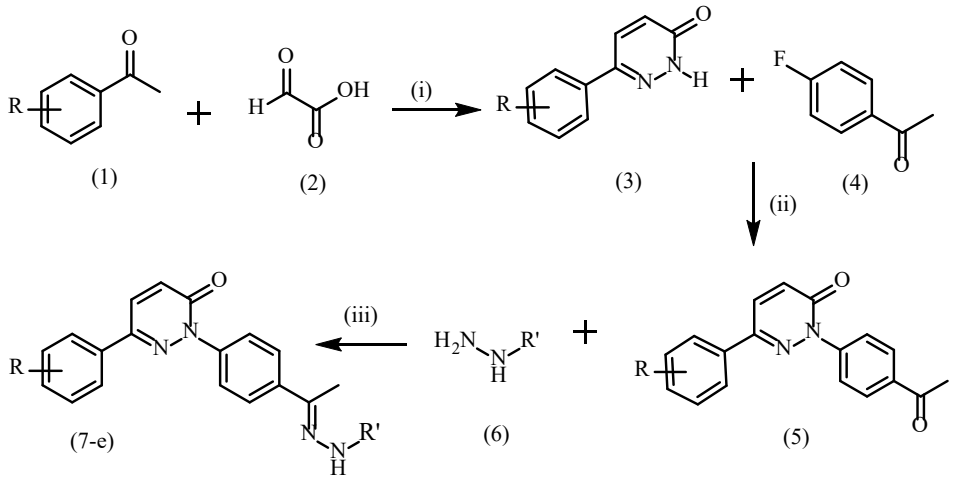

7a/7d: R = 4-methoxy/3-methoxy R' = Benzohydrazide
7b/7e : R = 4-methoxy/3-methoxy R' = 4-phenylthiocarbazide
7c/7f : R = 4-methoxy/3-methoxy R' = *p*-toluenesulfonylhydrazide

FIGURE 1. Preparation of compounds **7a-f**. Reagents and conditions as state in Table 1

TABLE 1. Preparation of pyridazinone-hydrazone hybrids (**7a-f**) at each stage of the reaction

Stage	Reaction condition	Solvent	Temp/Time	Product
1	Glyoxylic acid (3 mmol), 4- methoxy acetophenone (3 mmol)	CH_3COOH (3 mL)	120 °C/ ± 3 hours	Compound **3**
2	Compound **3** (1 mmol), fluoroacetophenone (1.25 mmol)	K_2CO_3 (1 mmol) in DMSO (4 mL)	100 °C /16 hours	Compound **5**
3	compound **5** (1 mmol), hydrazide derivatives (4 mmol)	CH_3CH_2OH (5 mL), CH_3COOH (3 mL)	medium-low power/3-10 min	Compounds **7a-f**

hydrate to form the pyridazinone ring. This method renders the synthesis of pyridazinone derivatives more efficient and practical due to its solvent-free conditions, reduced reaction time, and minimisation of repetitive work-up steps (Cruz et al. 2016). Furthermore, the use of monowave irradiation presents an attractive alternative, as it provides uniform heating within a closed system (sealed vessels) (Obermayer et al. 2016). This accelerates the reaction and minimises compound degradation, ultimately leading to a higher yield and greater purity of the pyridazinone derivative products for 6 h (Yuni et al. 2025). The mechanism of the one-pot reaction of compound **3** is displayed in Figure 2.

In stage 2, compound **5** was synthesised via an aromatic nucleophilic substitution (SNAr) reaction (Barbasiewicz et al. 2023). The reaction mechanism begins with K_2CO_3 base catalysis, which takes hydrogen atoms from the N-H group, thereby increasing the nucleophilicity of the nitrogen atom. Next, the nucleophilic nitrogen attacks the partially positive carbon atom in the C-F bond, resulting in the formation of the active Meisenheimer complex intermediate. In the final stage, the F group is released, forming compound **5**. The substitution of the acetophenone moiety was confirmed by ^{1}H-NMR spectroscopy, where the NH proton signal on the pyridazinone ring was missed. Instead, new signals due to the protons and carbons of the acetophenone moieties were noticed.

In stage 3, compound **5** was reacted with various hydrazines to yield new hydrazone derivatives **7a-f** via an addition-elimination mechanism. The carboxylic acid catalyst serves as a resonance-stabilised enolate species to increase the electrophilic properties of the carbonyl group, making it more reactive to nucleophilic attack. Then, the primary amine nucleophile, in this case the amine in the hydrazide derivatives, will attack the electrophile so that the reaction equilibrium will shift towards the formation of the imine product (Schiff base), followed by a condensation reaction or elimination of the by-product H_2O. In this study, the product is also called a hydrazone with the general structure $R_1R_2C{=}NNH_2$ because it is formed as a reaction between a hydrazine and ketone/aldehyde (Fazal et al. 2020). It is important to emphasise that the process was carried out within a short reaction

time of 3-10 min. In contrast to the method previously reported by Can et al. (2017) and Kamat et al. (2024) which required 24-36 h of reflux to obtain the hydrazone product. This study demonstrates that the use of moderate-energy microwave irradiation significantly accelerates the formation of compound **7**. This finding highlights the novelty of the microwave-assisted approach in enhancing reaction efficiency to obtain hydrazone derivatives. The reaction mechanism of **7a-f** is shown in Figure 3. FT-IR spectroscopy analysis of compounds **7a-f** shows that the appearance of an N-H stretching band (3247-3349 cm^{-1}) is the most important indicator of the successful synthesis of compound **5** into compounds **7**.

MOLECULAR DOCKING ENZIM α-GLUCOSIDASE

In this study, the α-glucosidase enzyme from *Saccharomyces cerevisiae* (PDB ID: 3A4A, 1.60 Å) was selected as the target receptor. This enzyme is specifically an oligo-1,6-glucosidase that has isomaltase activity (Yamamoto et al. 2010). Target validation for docking simulations is supported by homology studies. The high sequence similarity (71.92-84%) between α-glucosidase (MAL12; 584 AS) from *S. cerevisiae* (Swiss-Prot: P53341) and the crystal structure of oligo-1,6-glucosidase (3A4A; 589 AS) establishes 3A4A a valid template (Syahrul et al. 2015; Wening et al. 2017). As the established standard for *in vitro* α-glucosidase inhibition assays, the significance of this enzyme is reinforced by the robust correlation between *in silico* docking studies (using structure 3A4A) and experimental data, confirming the reliability of this combined approach in predicting bioactivity (Guerreiro et al. 2013; Liu et al. 2020; Peytam et al. 2021).

The docking protocol was obtained by redocking the native ligand isomaltose. The redocking results showed a value of S = -7.72 kcal/mol and RMSD = 1.78 Å. A docking protocol with an RMSD value < 2 is considered valid, so it can be used as a docking method for target ligands. The RMSD value indicates the deviation that occurs during docking, where the smaller the RMSD value,

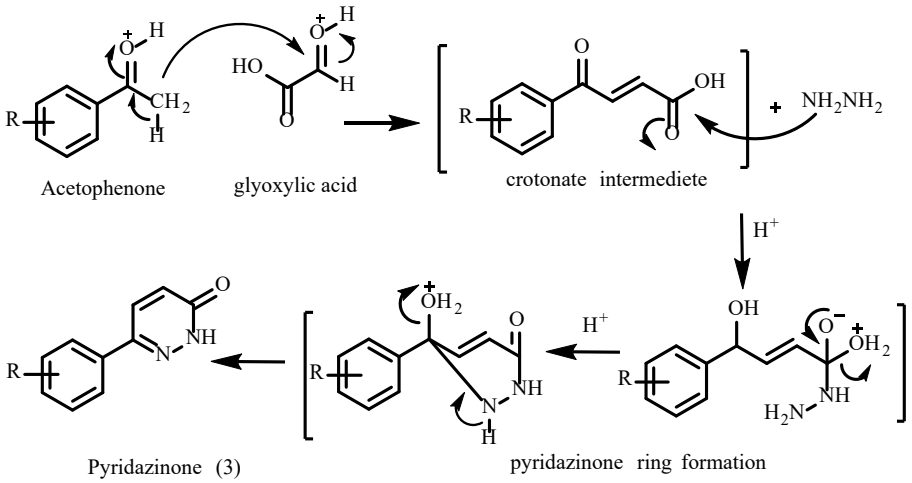

FIGURE 2. The reaction mechanism of compound **3**

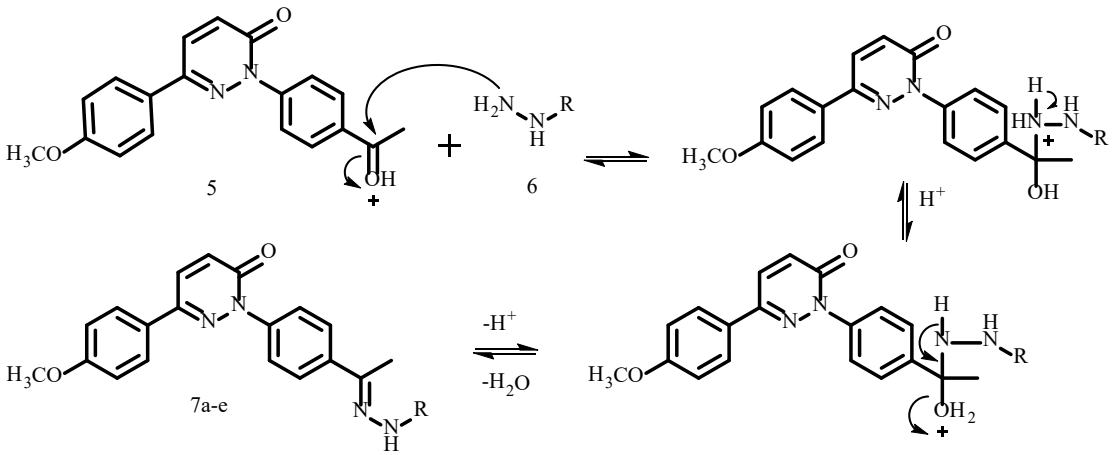

FIGURE 3. The reaction mechanism of **7a-f**

the smaller the error deviation in performing docking. This means that the position of the redocking ligand is similar to the position of the native ligand (Neni, Benni & Regina 2019). The smaller the average RMSD of the best-ranked pose, the better the performance of the scoring function or scoring model (Zheng et al. 2022).

According to Sim et al. (2008), important residues, such as His112, Asp215, Glu277, His351, and Asp352, are involved in glycosidic bond cleavage. The role of Asp is crucial because it is required in glycosidic bond cleavage (glycosylation and deglycosylation). Acarbose, as a positive control, has an S value of -9.59 kcal/mol and forms 7 hydrogen bonds with important residues. All pyridazinone derivatives exhibited S values close to that of acarbose, with compound **7c** (-8.97 kcal/mol) demonstrating the most comparable binding affinity. They also interact to form hydrogen bonds and hydrophobic bonds with residues. The binding free energy values and interactions of each α-glucosidase enzyme ligand-receptor complex (ID **3A4A**) are presented in Table 2 and Figure 4.

Based on the molecular docking results, the binding affinity of the synthesized compounds was observed to

TABLE 2. Binding free energy and ligand interaction with active site of α-Glucosidase enzyme (3A4A)

Compounds	BFE (kkal/mol)	RMSD	Type of Chemical Bound		Residue Contact	interaction
			Hydrogen bound	Vand der Waals		
7a	-7.48	1.87	Asp352	Arg315, Phe314, Glu277	Arg213, **Arg315, Arg442, Asp215**, Asp233, **Asp307, Asp352, Asp69, Gln279, Glu277, Glu411, His351, Leu313,** Lys156, **Phe159, Phe178, Phe303, Phe314, Pro312, Ser240, Ser311, Thr310, Tyr158, Tyr72, Val216**	23
7b	-7.88	0.95	Asp362	Arg315, Phe314	**Arg315**, **Arg442**, **Asp215**, Asp233, **Asp307**, **Asp352**, **Asp69**, Gln182, Gln239, Gln279, **Glu277**, **Glu411**, **His112**, **Leu313**, Lys156, **Phe159**, **Phe178**, **Phe303**, **Phe314**, **Pro312**, **Ser240**, **Ser311**, Thr310, **Tyr158**, **Tyr72**, **His351**, **Val216**, Val232	22
7c	-8.97	1.31	Lys156	Glu277, Tyr158	**Arg315, Arg442, Asn415, Asp215, Asp352, Asp69**, Gln182, Gln353, **Glu277, Glu411, His112, Leu313,** Lys156, **Phe159**, **Phe178, Phe303, Phe314, Pro312,** Ser157, **Ser240**, Ser241, **Tyr158, Tyr316, Tyr72**	19
7d	-7.43	1.54	Thr310	Arg315	**Glu277**, **Arg442**, Val308, **Pro312**, Thr310, **Ser311**, **Asp307**, Ser304, **Phe314**, **Arg315**, **Phe303**, **His280**, **Phe159**, **Glu411**, **Tyr158**, **Asp352**	13
7e	-7.86	1.90	Asp352, Arg315	His280	**Phe159**, Gln182, **Phe303**, **Tyr158**, Asp69, **Gln279**, **His280**, **Asp307**, **Asp242**, **Phe314**, **Arg315**, **Glu411**, **Ser311**, **Pro312**, **Phe178**, **Tyr72**, **Asp215**, **Glu277**, **Leu313**, **His112**, **Val216**, **Arg442**, **Asp352**, **His351**	22
7f	-7.46	1.59	Glu411, Lys156	-	Thr306, **Phe178**, **Asp307**, **Arg315**, **His280**, **Tyr158**, **Ser240**, **Leu313**, **Asp242**, **Pro312**, Lys156, **Glu411**, **Asn415**, **Arg442**, **Asp352**, Gln353, **Tyr316**, **Phe159**, **Phe303**.	16
acarbose	-9,59	1,74	Glu277, Gln279, Asp242, Pro312, Glu411, Glu411, Arg442		Arg315, Arg442, Arg446, Asn415, Asp215, Asp242, Asp307, Asp352, Asp69, Gln279, Glu277, Glu411, His112, His280, His351, Leu313, Phe159, Phe178, Phe303, Phe314, Pro312, Ser240, Ser311, Tyr158, Tyr316, Tyr72, Val216	27

*Bold is the same amino acid that bind with the positive control

be influenced by the position of the methoxy substituent on the phenyl ring. In all cases, the 4-methoxy isomers demonstrated slightly stronger binding affinities than their 3-methoxy counterparts: **7a** (7.48 kcal/mol) > **7d** (7.43 kcal/mol), **7b** (7.88 kcal/mol) > **7e** (7.86 kcal/mol), and **7c** (7.89 kcal/mol) > **7f** (7.62 kcal/mol). This suggests that for these particular derivatives, the *para* position is more favorable for interaction with the active site of the enzyme. However, a contrasting trend was observed for compound **7c** (4-methoxy isomer), where demonstrated a significantly strongest binding affinity (-8.97 kcal/mol) among them. This indicates that the effect of the methoxy position is uniform and may be dependent on the overall molecular structure of the core scaffold.

In another supporting observation, the structure of acarbose, which has a large molecular weight, extends along the C-terminal side of the barrel domain A to the entrance of the active site pocket. The structure of compounds **7a-f** also extends to occupy the active site of the receptor, similar to the position of acarbose, because it has a large molecular weight. The active site pocket on the C-terminal side of barrel domain A contains the catalytic residues Asp215, Glu277, and Asp352, and the entrance to the active site pocket contains the residues Tyr158, His280, and loop 310–315. Therefore, this spread region allows compounds **7a-f** to have better inhibitory activity with multiple residue contacts. Identification of residue contact is also one of the crucial factors that can influence the affinity and level of inhibitory activity of a ligand towards a receptor. Observable binding sites can include well-known interaction patterns (such as hydrogen bonds and Van der Waals) and ligand atoms interacting without patterns (the remainder had no direct interactions) (Kasahara, Shirota & Kinoshita 2013). Visualisation of the spread orientation of the compounds **7a-f** ligand structures on the active side of the enzyme is shown in Figure 5.

DENSITY FUNCTIONAL THEORY (DFT)

Density Functional Theory (DFT) calculations were performed on the best conformations predicted by molecular docking for each compound. The DFT results consisted of total energy, HOMO and LUMO energies, energy gap, and dipole moment (Table 3). The total energy calculation indicated the thermodynamic stability of the molecule. The most stable structural state was characterised by the lowest bond free energy (Asiri et al. 2011). Among compounds **7a-7f**, compound **7c** exhibited the lowest total energy (-1923.18 Hartree), confirming it as the most stable structure in this series. However, acarbose demonstrated greatest stability

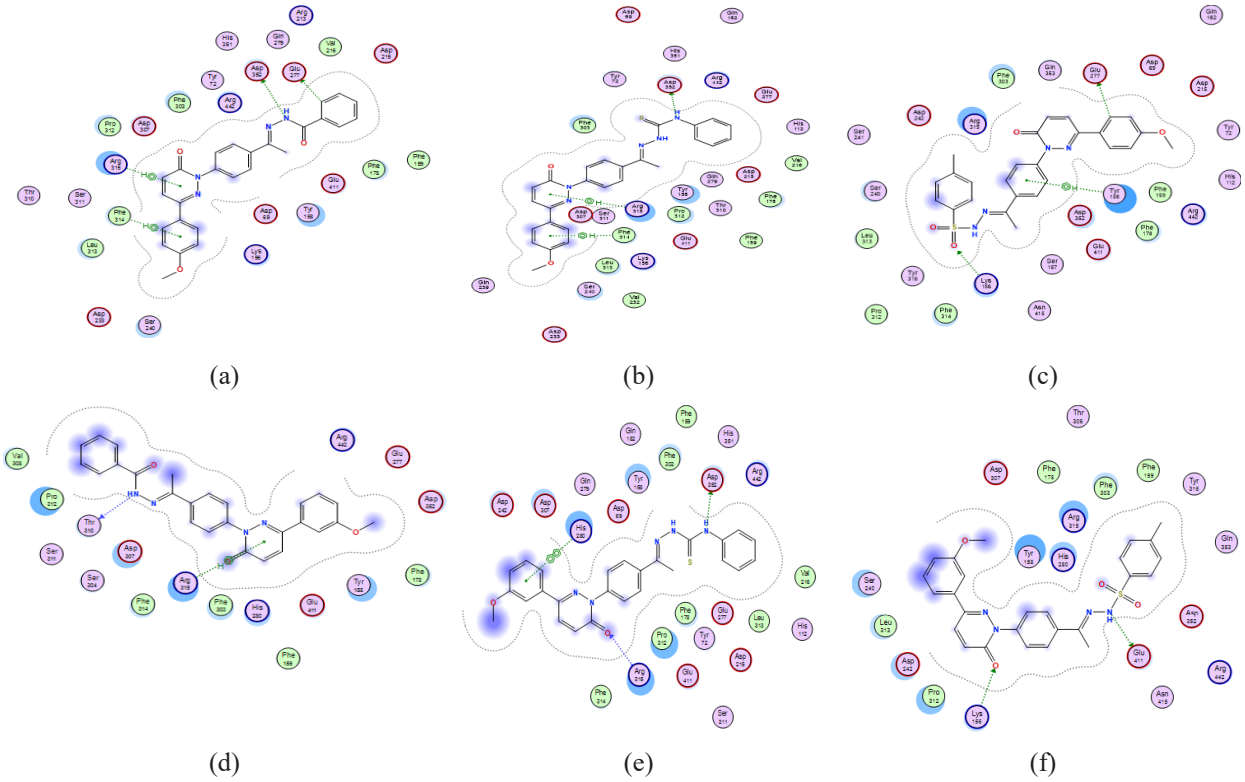

FIGURE 4. 2D visualisation of the interaction between ligands and the α-glucosidase enzyme receptor (ID **3A4A**): (a) **7a**; (b) **7b**; (c) **7c**; (d) **7a**; (e) **7b**; (f) **7c**

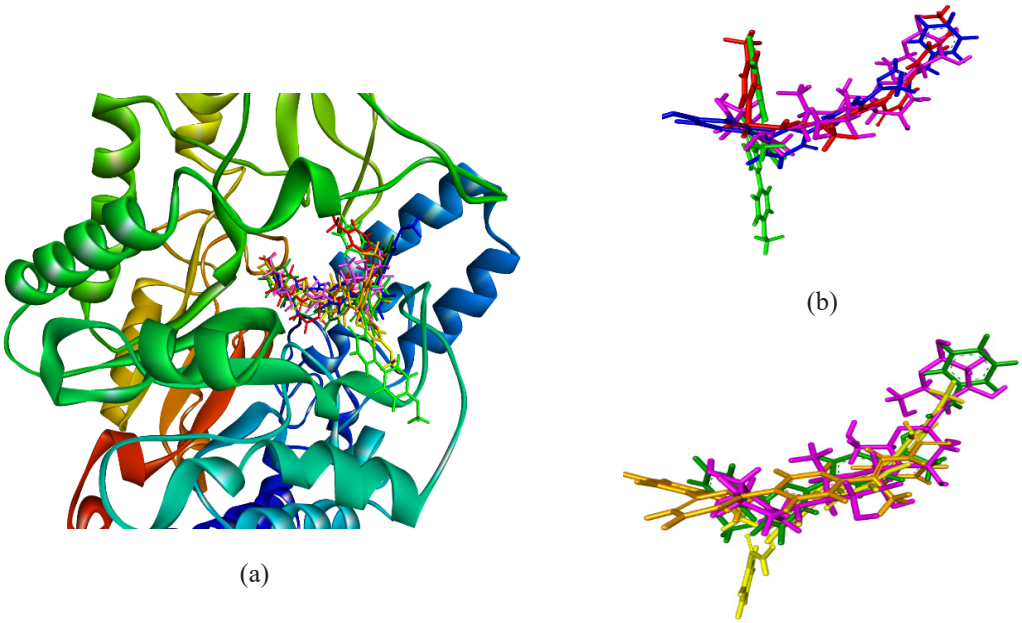

(a) (b) (c)

FIGURE 5. Visualization of the orientation of the ligand structures in the active site of the enzyme: a) **7a** (green), **7b** (blue), **7c** (red); (b) yellow (**7d**), deep green (**7e**), orange (**7f**), acarbose (pink)

among all the synthesized compounds. Furthermore, in the same analysis as the docking energy stability results, it was found that the total energy order from the DFT results was **7a** < **7d**, **7b** < **7e**, and **7c** < **7f**. This indicates that the 4-methoxy isomers are thermodynamically more stable than their 3-methoxy counterparts. This suggests that for these particular derivatives, the position is more favorable for interaction with the active site of the enzyme.

HOMO and LUMO are fundamental concepts in organic chemistry for understanding the electronic properties and reactivity of a compound (Neni et al. 2025). HOMO is the highest-energy molecular orbital in the valence band occupied by electrons that represent the compound's ability to donate electrons (nucleophilic). Meanwhile, LUMO is the lowest-energy molecular orbital that is empty or not filled with electrons, representing an electron-deficient compound (electrophilic). The electronic transition obtained from the difference between the LUMO and HOMO energies (ΔE = HOMO-LUMO) is called the energy gap. Among all target compounds, **7e** exhibited the smallest HOMO-LUMO energy gap, followed by **7e** < **7f** < **7d** < **7b** < **7c** < **7a**. Conversely, the larger the energy gap value, the more stable and less reactive the molecule is because it requires a large amount of energy to undergo electron excitation from HOMO to LUMO (Asiri et al. 2011; Noureddine, Issaoui & Al-dossary 2021).

In addition to having the lowest total energy, acarbose also displays the largest HOMO-LUMO energy gap (0.20017 Hartree) among the tested compounds. This confirms that acarbose has the highest kinetic stability, further supporting its potential as a stable inhibitor. This is likely due to the fact that acarbose's inhibitory activity against the enzyme does not depend on electronic reactivity but rather on its ability to form non-covalent interactions (7 hydrogen bonds) with enzyme residues. In addition, acarbose has a rigid cyclic ring structure similar to the substrate (polysaccharide), so the structural similarity of acarbose to the substrate supports its bioactivity rather than its electronic reactivity.

Meanwhile, the target compound may work through a slightly different mechanism with acarbose. Furthermore, based on the dipole moment calculations, Compounds **7a-f** are predicted to be polar (dipole moment $\mu > 0$). The greater the dipole moment value, the more polar the compound. Compounds **7a-f** are polar because they contain polar functional groups such as NH_2, carbonyl, and SO_2, as well as a delocalised π electron system. Despite having a large number of hydroxyl groups in its structure, acarbose only has a dipole moment of 3.91 D. This value also indicates that acarbose is polar. The dipole moment of acarbose is lower compared to that of the target compound. This disparity is likely due to the steric shape and local symmetry of the acarbose structure, as obtained from the best conformational docking results, which may hinder or limit its polar interactions with water molecules. Therefore, the DFT calculation results show that the dipole moment of acarbose is smaller than theoretically predicted.

In compounds **7a-f**, the electron distribution in the HOMO orbitals is dominant on one side of the molecule or delocalised towards electronegative atoms (SO_2, oxygen,

and nitrogen atoms). This pattern indicates a charge imbalance, which contributes to the magnitude of the dipole moment and total energy values. This means that compounds **7a-f** are reactive.

Molecular electrostatic potential (MEP) shows the distribution of electron density and helps identify areas that are vulnerable to electrophilic and nucleophilic attacks, as well as the potential for hydrogen bonding interactions (Abbaz, Bendjeddou & Villemin 2018; Noureddine, Issaoui & Al-dossary 2021). In the target compound, the MEP graphical representation shows that nucleophilic (red) regions are localised around the methoxy, carbonyl, SO_2, and amine groups. These negatively charged regions play an important role in electrostatic interactions with positively charged residues in the active site of the receptor. Conversely, the electrophilic regions (blue) are located on the hydrogen atoms of NH, indicating that these hydrogen atoms can act as electron acceptors when interacting with electron donor groups from the amino acid residues of the receptor. MEP visualisation is displayed in Figure 6.

In vitro ANTIDIABETIC TEST USING THE α-GLUCOSIDASE INHIBITION METHOD

Based on molecular docking studies, which predicted stable binding affinities of compounds **7a-7f** toward the α-glucosidase enzyme, compounds **7a-7c** were subsequently selected for *in vitro* α-glucosidase inhibitory assays. The results showed that compounds **7a-7c** exhibited strong inhibitory activity against α-glucosidase, with the following order of potency: **7c** (IC_{50} = 12.35 µg/mL) > **7b** (IC_{50} = 18.80 µg/mL) > **7a** (IC_{50} = 26.33 µg/mL). The best activity exhibited by compound **7c** can be attributed to the presence of a sulfonylurea group within its structure. These results are consistent with previous studies, which have predicted that the combination of a pyridazinone scaffold with sulfonylurea groups represents a promising framework for the development of antidiabetic candidates (Faidallah et al. 2011; Kharbanda et al. 2015; Moghimi et al. 2020; Yuni et al. 2025). This assumption is also supported by molecular docking results showing that **7c** (-8.97 kcal/mol) demonstrated the most comparable binding affinity among

TABLE 3. Results of quantum chemical parameter calculations for pyridazinone-hydrazone hybrids (**7a-f**) using the B3LYP model / 6-31G (dp) basis set

Compounds	Total energy (Hartree)	µ (D)	Molecular orbital energy (Hartree)		GAP energy (Hartree)
			HOMO	LUMO	
10a	-1448.649	4.201	-0.214	-0.076	0.148
10b	-1826.966	8.129	-0.191	-0.074	0.127
10c	-1923.180	9.289	-0.217	-0.077	0.140
10d	-1431.677	5.072	-0.202	-0.303	0.101
10e	-1807.512	5.800	-0.202	-0.263	0.061
10f	-1902.627	8.901	-0.199	-0.288	0.089
acarbose	-2387.101	3.925	-0.210	-0.013	0.207

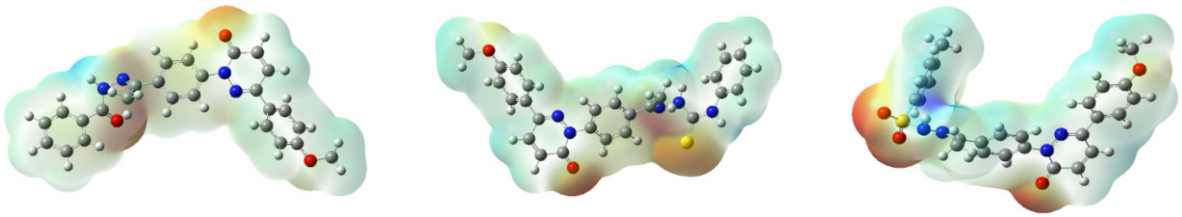

7a **7b** **7c**

FIGURE 6. MEP visualization was used DFT/ B3LYP/basis set 6-31G(dp) method: the red colour represents negative charges, while the blue represents positive charges

the derivatives. Furthermore, *in vitro* results also show that acarbose has very strong activity, which is also supported by docking predictions with the smallest S value and the ability to form 7 hydrogen bonds. According to Neni et al. (2017), the more hydrogen bond interactions formed between the ligand complex and the receptor, the more active the pharmacological activity of the ligand towards the receptor is predicted to be.

PHARMACOKINETIC PROFILE

In this study, ADMET profiling was performed using an *in silico* model based on pKCSM and served as an initial screening to anticipate drug failure caused by undesirable pharmacokinetic properties of compounds in drug candidate development (Shou 2020). The results showed that compounds **7a-f** were predicted to have good oral bioavailability, as they complied with Lipinski's rule of five, which suggests that such compounds are likely to be absorbed into the systemic circulation when administered orally (Neni et al. 2021). In this study, compounds **7a-f** have appropriate molecular weights (<500). Drug molecules with appropriate molecular weights will easily diffuse through cell membranes.

The logP values are within an acceptable range, indicating that the test compounds are slightly more nonpolar, enabling them to pass through the lipid bilayer membrane in accordance with their lipophilicity. This hydrophobic property is due to the large molecular weight of the molecule, where the contribution of the nonpolar part (three aromatic rings) is far more dominant in the overall partition behaviour. This is in line with the MEP visualisation, which shows that polarity is not distributed across the entire molecule but is localised to specific heteroatoms (N and O atoms). These findings suggest that the target compound is a promising candidate for drug development, with favourable predicted bioavailability. According to Rashid (2020), Lipinski's five rules methodology was used to analyse drug-likeness properties. These properties are defined as a complex balance of many properties and features of drug candidates.

In this study, acarbose has a very low logP value of-8.17, which indicates its highly hydrophilic nature. This rule comes from understanding that very low logP makes the drug difficult to penetrate the lipid bilayer of cell membranes and might affect its efficacy (Linda et al. 2022). It is known that Acarbose is poorly absorbed and is excreted in the feces, mostly intact, but with up to 30% undergoing metabolism predominantly via fermentation by colonic microbiota (Derosa & Maffioli 2012). Furthermore, we also found that these results are consistent with its zero HIA adsorption value and Caco-2 permeability value of -0.825, both of which confirm the absence of absorption and poor membrane penetration ability of acarbose.

Although the compound shows high predicted human intestinal absorption (HIA) of 90-95%, its low Caco-2 permeability value indicates that the rate of absorption into the enterocytes is very slow. The high HIA value may also be a potentially beneficial aspect. This indicates that only a small portion of the compound remains in the intestinal lumen, suggesting that compounds **7a-f** may cause milder gastrointestinal side effects compared to first-generation α-glucosidase inhibitors, such as acarbose, which has a low HIA value and acts locally in the intestine. Therefore, this hypothesis needs to be further validated through *in vitro* and *in vivo* testing of the intestinal microbiome to ensure that the small number of compounds remaining in the intestine is indeed correlated with good tolerance and eliminates direct irritation of the compounds on the intestine.

Pharmacokinetic drug-drug interactions occur when a drug is administered with another drug simultaneously so that it can change absorption, transportation, distribution, metabolism and excretion, which results in an increase or decrease in drug concentration, which can significantly affect the efficacy and safety of the drug in patients (Peng, Cheng & Xie 2021). Compounds **7a-f** are predicted to be metabolised by several cytochrome P450 (CYP) isoforms, suggesting a potential for drug-drug interactions (DDI) when co-administered with other drugs metabolised by the same enzymes. Previous studies have investigated the drug-drug interaction (DDI) between the antidepressant fluoxetine and gefitinib. Fluoxetine exhibits a strong inhibitory effect on the CYP2D6 isoenzyme, whereas the therapeutic activity of gefitinib in lung cancer has been linked to metabolism by this same enzyme. This study found that fluoxetine exerts an inhibitory effect on the metabolism of gefitinib via the CYP2D6 isoenzyme. This inhibition of cytochrome P450 may lead to pharmacokinetic alterations and a subsequent reduction in the efficacy of gefitinib as a cancer treatment (Luong et al. 2021). Additionally, consistent with the hepatotoxicity prediction, the extensive first-pass metabolism in the liver could generate oxidative stress and lead to hepatocellular injury, especially during prolonged administration. DILI is one of the main reasons for the rejection or withdrawal of a drug/drug candidate from the market by the pharmaceutical industry (Jiang et al. 2019). Although all compounds exhibited predicted hepatotoxicity, compounds **7c** and **7f** demonstrated a better safety profile, as they were the only non-mutagenic derivatives. Therefore, these two compounds may be considered promising candidates for further optimisation to reduce hepatotoxicity while retaining their non-mutagenic properties.

The total clearance value of the target compound is also quite high (i.e., rapidly cleared from the systemic circulation). Furthermore, the moderate VDss values predicted for compounds **7a-f** indicate that they might not be tightly bound to plasma proteins, potentially facilitating tissue distribution and receptor interaction (Singh, Kapoor & Bhatnagar 2021). The blood-brain barrier (BBB) values of compounds **7a-f** predicted that the test compounds would be distributed across the BBB, although not at high levels. The BBB functions as a homeostasis maintenance and defence system that regulates the exchange of

TABLE 4. ADMET profile of pyridazinone-hydrazon hybrids (**7a-f**) via pKCSM and ProTox II

ADMET Profiles	**7a**	**7b**	**7c**	**7d**	**7e**	**7f**	akarbosa	standard
Lipinski's rule of five								
Molecular Weight	438	470	488	438	470	488	645	≤ 500
Hydrogen Bond Donor	1	2	1	1	2	1	14	≤ 5
Hydrogen Bond Acceptor	7	7	7	6	7	7	19	≤10
LogP	4.45	5.24	5.39	4.45	5.08	5.39	-8.17	≤ 5
Adsorption								
HIA (%)	96.2	90.5	95.6	97.0	94.1	95.6	0	poor (< 30 %)
Caco-2 cell permeability (log Papp dalam 10^{-6}cm/s)	0.69	0.57	0.59	0.69	0.80	0.59	-0.82	high permeability (0,90)
skin permeability: log Kp (cm/h)	-2.72	-2.73	-2.73	-2.72	-2.73	-2.73	-2.73	low (log Kp > -2,5)
Distribution								
VDSS (human) (logL/kg)	-0.14	-0.18	-0.14	-0.09	-0.03	-0.13	-0.80	low (< -0,15), High (Log > 0,45)
Blood Brain Barrier (log BB) [d]	-0,52	-0.77	-0.91	-0.15	-0.49	-0.91	-3	able to pass through the membrane (logBB > 0,3) dan less distributed (log BB < -1)
CNS permeability (log PS)	-2.03	-2.39	-2.31	-2.04	-1.95	-2.31	-7.8	penetration (log PS > -2). Not penetration (log PS < -3)
Metabolism								
CYP2D6 Substrate	No	Yes	No	No	Yes	No	No	No/Yes
CYP3A4 Substrate	Yes	Yes	Yes	Yes	Yes	Yes	No	No/Yes
CYP1A2 Inhibitor	No	Yes	No	Yes	Yes	No	No	No/Yes
CYP2C19 Inhibitor	Yes	Yes	Yes	Yes	Yes	Yes	No	No/Yes
CYP2C9 Inhibitor	Yes	Yes	Yes	Yes	Yes	Yes	No	No/Yes
CYP2D6 Inhibitor	No	No	No	No	No	No	No	No/Yes
CYP3A4 Inhibitor	Yes	Yes	Yes	Yes	Yes	Yes	No	No/Yes
Excretion								
total clearance	0.61	062	0.22	0.62	-0.21	0.21	0.5	The higher the better
Renal OCT2 substrate	No	No	No	No	No	No	No	No/Yes
Toxicity								
Ames toxicity	Yes	Yes	No	Yes	Yes	No	No	No/Yes
hepatotoxicity	Yes	Yes	Yes	Yes	Yes	Yes	No	No/Yes
skin sensitization	No	No	No	No	No	No	No	No/Yes
oral acute toxicity (LD50) (mg/kg)	2000	564	1000	1000	1000	1000	24000	
Kelas*	4	4	4	4	4	4	6	

molecules from the blood to the brain. Meanwhile, the CNS permeability (log PS) values of compounds **7a-f** are in the zone indicating very low permeability (very difficult to penetrate) in optimal time. As a result, pharmacologically, it is very difficult for them to reach effective concentrations in the brain. This is likely due to the lipophilic and large molecular weight of drug targets, which slows down the rate of partition into the brain (Rankovic 2014). Conversely, they may be good candidates for drugs that are not targeted to the CNS, especially drugs for inhibitors α-glukosidase.

As part of the comprehensive profile of the oral antidiabetic drug candidate, this compound exhibited moderate skin permeability and did not cause skin sensitisation, providing additional information regarding

its safety characteristics. Further prediction results indicate that none of the test compounds are substrates of OCT2, which is a favourable indicator in terms of drug safety. As OCT2 serves as the primary elimination pathway for many cationic drugs such as metformin, the absence of OCT2 substrate activity may minimise the potential for unwanted competitive drug interactions, thereby reducing the risk of toxicity (Koepsell 2021). The lower the LD_{50} value, the higher the toxicity level of a compound. Conversely, the higher the LD_{50} value, the safer the compound. Based on the LD_{50} value, test compounds with values ranging from 300 to 5000 mg/kg (classes 4 and 5) are generally considered to have low acute oral toxicity.

CONCLUSIONS

New pyridazinone–hydrazone hybrids (**7a-f**) were synthesized efficiently via microwave irradiation, yielding satisfactory results, and were validated through UV, FTIR, HRMS, ^{1}H-NMR, and ^{13}C-NMR studies. Molecular docking indicated favorable binding energies akin to acarbose, corroborated by DFT studies demonstrating advantageous electronic characteristics. *In vitro* studies demonstrated that compounds **7a-c** displayed significant α-glucosidase inhibitory activity, with IC_{50} values of 26.33, 18.80, and 12.35 µg/mL, respectively. While these findings underscore their potential as α-glucosidase inhibitors, ADMET predictions indicate constraints in oral bioavailability, such as diminished Caco-2 permeability and potential impacts from cytochrome P450 metabolism. Consequently, additional structure-activity relationship (SAR) investigations are necessary to enhance these compounds and their pharmacokinetic characteristics.

ACKNOWLEDGEMENTS

We would like to express our gratitude to the Chemistry Department, University of Riau, through the Ministry of High Education, Sciences, and Technology (KEMENDITISAINTEK) in Fundamental Research Scheme 2025, which has provided funding and facilities for this research under the research contract number: 102/C3/DT.05.00/PL/2025; 19536/UN19.5.1.3/AL.04/2025.

REFERENCES

Abbaz, T., Bendjeddou, A. & Villemin, D. 2018. Molecular structure, HOMO, LUMO, MEP, natural bond orbital analysis of benzo and anthraquinodimethane derivatives. *Pharmaceutical and Biological Evaluations* 5(2): 27-39. https://doi.org/10.26510/2394-0859.pbe.2018.04

Abdolrahimi, A., Woite, P., Kretschmar, K., Roemelt, M., Braun, T. & He, O. 2025. Sequential one-pot *N*-alkylation and aminocarbonylation of primary amines catalyzed by heterobimetallic Ir/Pd complexes. *Chem. Sci.* 16: 19414-19422. https://doi.org/10.1039/d5sc03892h

Abida Khan, Anupama Diwan, Hamdy K. Thabet & Mohd Imran. 2020. Synthesis of novel *N*-substitutedphenyl-6-oxo-3-phenylpyridazine derivatives as cyclooxygenase-2 inhibitors. *Drug Development Research* 81(5): 573-584. https://doi.org/10.1002/ddr.21655

Abuelizz, H.A., Iwana, N.A.N.I., Ahmad, R., Anouar, E.H., Marzouk, M. & Al-Salahi, R. 2019. Synthesis, biological activity and molecular docking of new tricyclic series as α-glucosidase inhibitors. *BMC Chemistry* 13(1): 52. https://doi.org/10.1186/s13065-019-0560-4

Ahmed, Eman M., Asmaa E. Kassab, Afaf A. El-Malah & Marwa S.A. Hassan. 2019. Synthesis and Biological Evaluation of Pyridazinone Derivatives as Selective COX-2 Inhibitors and Potential Anti-Inflammatory Agents. *European Journal of Medicinal Chemistry* 171: 25–37. https://doi.org/10.1016/j.ejmech.2019.03.036

Akdağ, M., Özçelik, A.B., Demir, Y. & Beydemir, S. 2022. Design, synthesis, and aldose reductase inhibitory effect of some novel carboxylic acid derivatives bearing 2-substituted-6-aryloxo-pyridazinone moiety. *Journal of Molecular Structure* 1258: 132675. https://doi.org/10.1016/j.molstruc.2022.132675

Altıntop, M.D., Demir, Y., Türkeş, C., Öztürk, R.B., Cantürk, Z., Beydemir, Ş. & Özdemir, A. 2023. A new series of hydrazones as small-molecule aldose reductase inhibitors. *Archiv Der Pharmazie* 356(4): 202200570. https://doi.org/10.1002/ardp.202200570

Asiri, A.M., Karabacak, M., Kurt, M. & Alamry, K.A. 2011. Synthesis, molecular conformation, vibrational and electronic transition, isometric chemical shift, polarizability and hyperpolarizability analysis of 3-(4-methoxy-phenyl)-2-(4-nitro-phenyl)-acrylonitrile: A combined experimental and theoretical analysis. *Spectrochimica Acta - Part A: Molecular and Biomolecular Spectroscopy* 82(1): 444-455. https://doi.org/10.1016/j.saa.2011.07.076

Assila, Hamza, Silvia A. Brandán, Salma Mortada, Younes Zaoui, Abdullah Yahya Abdullah Alzahrani, Suhana Arshad, Youssef Ramli, My El Abbes Faouzi, Khalid Karrouchi & M'hammed Ansar. 2024. Pyridazine Derivative as Potent Antihyperglycemic Agent: Synthesis, Crystal Structure, α-Amylase and α-Glucosidase Inhibition and Computational Studies. *Journal of Molecular Structure* 1308 (November 2023). https://doi.org/10.1016/j.molstruc.2024.138145

Barbasiewicz, M., Fedoryński, M., Loska, R. & Makosza, M. 2023. Analogy of the reactions of aromatic and aliphatic π-electrophiles with nucleophiles. *Molecules* 28(10): 4015. https://doi.org/https://doi.org/10.3390/molecules28104015

Can, N.Ö., Osmaniye, D., Levent, S., Sağlik, B.N., Inci, B., Ilgin, S., Özkay, Y. & Kaplancikli, Z.A. 2017. Synthesis of new hydrazone derivatives for MAO enzymes inhibitory activity. *Molecules* 22(8): 1381. https://doi.org/10.3390/molecules22081381

Chaudhry, Faryal, Abdul Qayuum Ather, Mohammad Javaid Akhtar, Ayesha Shaukat, Mohammad Ashraf, Mariya al-Rashida, Munawar Ali Munawar & Misbahul Ain Khan. 2017. Green Synthesis, Inhibition Studies of Yeast α-Glucosidase and Molecular Docking of Pyrazolylpyridazine Amines. *Bioorganic Chemistry* 71: 170–80. https://doi.org/10.1016/j.bioorg.2017.02.003

Cruz, S., Cifuentes, D., Hurtado, N. & Román, M. 2016. Síntesis de piridazin-3(2H)-onas asistida por microondas en condiciones libre de disolvente. *Informacion Tecnologica* 27(5): 57-62. https://doi.org/10.4067/S0718-07642016000500007

Derosa, G. & Maffioli, P. 2012. α-glucosidase inhibitors and their use in clinical practice. *Archives of Medical Science* 8(5): 899-906. https://doi.org/10.5114/aoms.2012.31621

Drwal, Malgorzata N., Priyanka Banerjee, Mathias Dunkel, Martin R. Wettig, & Robert Preissner. 2014. ProTox: A Web Server for the in Silico Prediction of Rodent Oral Toxicity. *Nucleic Acids Research* 42 (W1): 53–58. https://doi.org/10.1093/nar/gku401

Dundar, Yasemin, Ozge Kuyrukcu, Gokcen Eren, F. Sezer Senol Deniz, Tijen Onkol & Ilkay Erdogan Orhan. 2019. Novel Pyridazinone Derivatives as Butyrylcholinesterase Inhibitors. *Bioorganic Chemistry* 92 (September). https://doi.org/10.1016/j.bioorg.2019.103304

Faidallah, Hassan M, Khalid A Khan & Abdullah M Asiri. 2011. Synthesis and Biological Evaluation of New 3-Trifluoromethylpyrazolesulfonyl-Urea and Thiourea Derivatives as Antidiabetic and Antimicrobial Agents. *Journal of Fluorine Chemistry* 132 (2): 131–37. https://doi.org/10.1016/j.jfluchem.2010.12.009

Fazal Rahim, Khalid Zaman, Muhammad Taha, Hayat Ullah, Mehreen Ghufran, Abdul Wadood, Wajid Rehman, Nizam Uddin, Syed Adnan Ali Shah, Muhammad Sajid, Faisal Nawaz & Khalid Mohammed Khan. 2020. Synthesis, *in vitro* alpha-glucosidase inhibitory potential of benzimidazole bearing *bis*-schiff bases and their molecular docking study. *Bioorganic Chemistry* 94: 103394. https://doi.org/10.1016/j.bioorg.2019.103394

Firoozpour, Loghman, Faraz Kazemzadeh Arasi, Mahsa Toolabi, Setareh Moghimi, Maryam Armandeh, Farzaneh Salmani & Roya Pakrad 2023. Design, Synthesis and α-Glucosidase Inhibition Study of Novel Pyridazin-Based Derivatives. *Medicinal Chemistry Research* 32 (4): 713–22. https://doi.org/10.1007/s00044-023-03027-9

Guerreiro, L.R., Carreiro, E.P., Fernandes, L., Cardote, T.A.F., Moreira, R., Caldeira, A.T., Guedes, R.C. & Burke, A.J. 2013. Five-membered iminocyclitol α-glucosidase inhibitors: Synthetic, biological screening and *in silico* studies. *Bioorganic and Medicinal Chemistry* 21(7): 1911-1917. https://doi.org/10.1016/j.bmc.2013.01.030

Hafiza Zara Tariq, Aamer Saeed, Saeed Ullah, Noor Fatima, Sobia Ahsan Halim, Ajmal Khan, Hesham R. El-Seedi, Muhammad Zaman Ashraf, Muhammad Latif & Ahmed Al-Harrasi. 2023. Synthesis of novel coumarin-hydrazone hybrids as α-glucosidase inhibitors and their molecular docking studies. *RSC Advances* 13(37): 26229-26238. https://doi.org/10.1039/d3ra03953f

Hedrington, M.S. & Davis, S.N. 2019. Considerations when using α-glucosidase inhibitors in the treatment of type 2 diabetes. *Expert Opinion on Pharmacotherapy* 20(18): 2229-2235. https://doi.org/10.1080/14656566.2019.1672660

Jiang, Jian, Charlie D. Pieterman, Gökhan Ertaylan, Ralf L.M. Peeters & Theo M.C.M. de Kok. 2019. The Application of Omics-Based Human Liver Platforms for Investigating the Mechanism of Drug-Induced Hepatotoxicity in Vitro. *Archives of Toxicology* Vol. 93. Springer Berlin Heidelberg. https://doi.org/10.1007/s00204-019-02585-5

Kamat, V., Venuprasad, K.D., Shadakshari, A.J., Bhat, R.S., D'Souza, A., Chapi, S., Kumar, A., Vijaykumar, P., Sankaranarayanan, M. & Venugopala, K.N. 2024. Synthesis, anti-inflammatory, antibacterial, and antioxidant evaluation of novel pyrazole-linked hydrazone derivatives. *Journal of Molecular Structure* 1312(Part 1): 138634. https://doi.org/10.1016/j.molstruc.2024.138634

Kasahara, Kota, Matsuyuki Shirota & Kengo Kinoshita. 2013. Comprehensive Classification and Diversity Assessment of Atomic Contacts in Protein-Small Ligand Interactions. *Journal of Chemical Information and Modeling* 53 (1): 241–48. https://doi.org/10.1021/ci300377f

Keri, R.S., Patil, M.R., Patil, S.A. & Budagupi, S. 2015. A comprehensive review in current developments of benzothiazole-based molecules in medicinal chemistry. *European Journal of Medicinal Chemistry* 89: 207-251. https://doi.org/10.1016/j.ejmech.2014.10.059

Kharbanda, Chetna, Mohammad Sarwar Alam, Hinna Hamid, Kalim Javed, Abhijeet Dhulap, Sameena Bano & Yakub Ali. 2015. Antidiabetic Effect of Novel Benzenesulfonylureas as PPAR-γ Agonists and Their Anticancer Effect. *Bioorganic and Medicinal Chemistry Letters* 25 (20): 4601–5. https://doi.org/10.1016/j.bmcl.2015.08.062

Khokra, Sukhbir Lal, Shah Alam Khan, Pramila Thakur, Deepika Chowdhary, Aftab Ahmad & Asif Husain. 2016. Synthesis, Molecular Docking and Potential Antioxidant Activity of Di/Trisubstituted Pyridazinone Derivatives. *Journal of the Chinese Chemical Society* 63 (9): 739–50. https://doi.org/10.1002/jccs.201600051

Koepsell, H. 2021. Update on drug-drug interaction at organic cation transporters: Mechanisms, clinical impact, and proposal for advanced *in vitro* testing. *Expert Opinion on Drug Metabolism & Toxicology* 17(6): 635-654. https://doi.org/10.1080/17425255.2021.1915284

Lebovitz, H.E. 1997. Alpha-glucosidase inhibitors. *Endocrinology and Metabolism Clinics of North America* 26(3): 539-551. https://doi.org/10.1016/S0889-8529(05)70266-8

Linda Ekawati, Beta Achromi Nurohmah, Jufrizal Syahri & Bambang Purwono. 2022. Substituted 3-styryl-2-pyrazoline derivatives as an antimalaria: Synthesis, *in vitro* assay, molecular docking, druglikeness analysis, and ADMET prediction. *Sains Malaysiana* 51(10): 3215-3236. https://doi.org/http://doi.org/10.17576/jsm-2022-5110-09

Liu, Y., Zhan, L., Xu, C., Jiang, H., Zhu, C., Sun, L., Sun, C. & Li, X. 2020. α-glucosidase inhibitors from Chinese bayberry (*Morella rubra* Sieb. et Zucc.) fruit: Molecular docking and interaction mechanism of flavonols with different B-ring hydroxylations. *RSC Advances* 10(49): 29347-29361. https://doi.org/10.1039/d0ra05015f

Luong, T-L.T., Mcanulty, M.J., Evers, D.L., Reinhardt, B.J. & Weina, P.J. 2021. Pre-clinical drug-drug interaction (DDI) of gefitinib or erlotinib with cytochrome P450 (CYP) inhibiting drugs, fluoxetine and/or losartan. *Current Research in Toxicology* 2: 217-224. https://doi.org/10.1016/j.crtox.2021.05.006

Moghimi, Setareh, Mahsa Toolabi, Somayeh Salarinejad, Loghman Firoozpour, Seyed Esmaeil Sadat Ebrahimi, Fatemeh Safari, Somayeh Mojtabavi, Mohammad Ali Faramarzi & Alireza Foroumadi. 2020. Design and Synthesis of Novel Pyridazine N-Aryl Acetamides: In-Vitro Evaluation of α-Glucosidase Inhibition, Docking, and Kinetic Studies. *Bioorganic Chemistry* 102 (June): 104071. https://doi.org/10.1016/j.bioorg.2020.104071

Nagle, Pramod, Yogesh Pawar, Atul Sonawane, Shyam Bhosale & Dhananjay More. 2014. Docking Simulation, Synthesis and Biological Evaluation of Novel Pyridazinone Containing Thymol as Potential Antimicrobial Agents. *Medicinal Chemistry Research* 23 (2): 918–26. https://doi.org/10.1007/s00044-013-0685-2

Neni Frimayanti, Benni Iskandar & Regina Dewi Putri. 2019. Docking studies of chalcone analogue compounds as inhibitors for breast cancer MCF7 cell line. *Der Pharma Chemica* 11(2): 31-35.

Neni Frimayanti, Abdi Wira Septama, Hilwan Yuda Teruna & Eldiza Puji Rahmi. 2025. *In silico* investigation of artocarpin, cycloarotcarpin, artocarpanone, and cyanomaclurin for dengue virus inhibitor DEN2 NS2B/NS3 serine protease. *Journal of Pharmacy and Pharmacognosy Research* 13(1): 193-202. https://doi.org/10.56499/jppres24.2052_13.1.193

Neni Frimayanti, Marzieh Yaeghoobi, Ihsan Ikhtiarudin, Dhea Rizki & Wannisyah Putri. 2021. Insight on the *in silico* study and biological activity assay molecular docking. *Chiang Mai University Journal of Natural Sciences* 20(1): e2021019.

Neni Frimayanti, Benni Iskandar, Marzieh Yaeghoobi, Heh Choon Han, Sharifuddin M Zain, Rohana Yusof & Noorsaadah Abdul Rahman. 2017. Docking, synthesis and bioassay studies of imine derivatives as potential inhibitors for dengue NS2B/NS3 serine protease. *Asian Pacific Journal of Tropical Disease* 7(12): 792-796.

Nidhar, M., Kumar, V., Mahapatra, A., Gupta, P., Yadav, B.K., Singh, R.K. & Tewari, A.K. 2023. Ligand-based designing of DPP-4 inhibitors via hybridization; synthesis, docking, and biological evaluation of pyridazine-acetohydrazides. *Molecular Diversity* 27(6): 2729-2740. https://doi.org/10.1007/s11030-022-10577-4

Noureddine, O., Issaoui, N. & Al-dossary, O. 2021. DFT and molecular docking study of chloroquine derivatives as antiviral to coronavirus COVID-19. *Journal of King Saud University - Science* 33(1): 101248. https://doi.org/10.1016/j.jksus.2020.101248

Obermayer, D., Znidar, D., Glotz, G., Stadler, A., Dallinger, D. & Kappe, C.O. 2016. Design and performance validation of a conductively heated sealed-vessel reactor for organic synthesis. *Journal of Organic Chemistry* 81(23): 11788-11801. https://doi.org/10.1021/acs.joc.6b02242

Pakkir Maideen, N.M. 2019. Pharmacologically relevant drug interactions of α glucosidase inhibitors. *Journal of Diabetes, Metabolic Disorders & Control* 6(2): 28-30. https://doi.org/10.15406/jdmdc.2019.06.00178

Peng, Y., Cheng, Z. & Xie, F. 2021. Evaluation of pharmacokinetic drug - Drug interactions: A review of the mechanisms, *in vitro* and *in silico* approaches. *Metabolites* 11(2): 75.

Peytam, F., Takalloobanafshi, G., Saadattalab, T., Norouzbahari, M., Emamgholipour, Z., Moghimi, S., Firoozpour, L., Bijanzadeh, H.R., Faramarzi, M.A., Mojtabavi, S., Rashidi-Ranjbar, P., Karima, S., Pakraad, R. & Foroumadi, A. 2021. Design, synthesis, molecular docking, and *in vitro* α-glucosidase inhibitory activities of novel 3-amino-2,4-diarylbenzo[4,5]imidazo[1,2-a]pyrimidines against yeast and rat α-glucosidase. *Scientific Reports* 11: 11911. https://doi.org/10.1038/s41598-021-91473-z

Rankovic, Z. 2014. CNS drug design: Balancing physicochemical properties for optimal brain exposure. *Journal of Medicinal Chemistry* 58(6): 2584-2608. https://doi.org/10.1021/jm501535r

Rashid, Mohammad. 2020. Design, Synthesis and ADMET Prediction of Bis-Benzimidazole as Anticancer Agent. *Bioorganic Chemistry* 96 (December 2019): 1–18. https://doi.org/10.1016/j.bioorg.2020.103576

Syahrul Imran, Muhammad Taha, Nor Hadiani Ismail, Syed Muhammad Kashif, Fazal Rahim, Waqas Jamil, Maywan Hariono, Muhammad Yusuf & Habibah Wahab. 2015. Synthesis of novel flavone hydrazones: *in-vitro* evaluation of α-glucosidase inhibition, QSAR analysis and docking studies. *European Journal of Medicinal Chemistry* 105: 156-170. https://doi.org/10.1016/j.ejmech.2015.10.017

Shayegan, N., Haghipour, S., Tanideh, N., Moazzam, A., Mojtabavi, S., Faramarzi, M.A., Irajie, C., Parizad, S., Ansari, S., Larijani, B., Hosseini, S., Iraji, A. & Mahdavi, M. 2023. Synthesis, *in vitro* α-glucosidase inhibitory activities, and molecular dynamic simulations of novel 4-hydroxyquinolinone-hydrazones as potential antidiabetic agents. *Scientific Reports* 13(1): 6304. https://doi.org/10.1038/s41598-023-32889-7

Shou, W.Z. 2020. Current status and future directions of high-throughput ADME screening in drug discovery. *Journal of Pharmaceutical Analysis* 10(3): 201-208. https://doi.org/https://doi.org/10.1016/j.jpha.2020.05.004

Sim, L., Quezada-Calvillo, R., Sterchi, E.E., Nichols, B.L. & Rose, D.R. 2008. Human intestinal maltase–glucoamylase: Crystal structure of the N-terminal catalytic subunit and basis of inhibition and substrate specificity. *Journal of Molecular Biology* 375(3): 782-792. https://doi.org/https://doi.org/10.1016/j.jmb.2007.10.069

Singh, M., Kapoor, A. & Bhatnagar, A. 2021. Physiological and pathological roles of aldose reductase. *Metabolites* 11(10): 655. https://doi.org/10.3390/metabo11100655

Teni Ernawati, Maksum Radji, Muhammad Hanafi, Abdul Mun'im & Arry Yanuar. 2017. Cinnamic acid derivatives as α-glucosidase inhibitor agents. *Indonesian Journal of Chemistry* 17(1): 151-160. https://doi.org/10.22146/ijc.23572

Wening Lestari, Rizna Triana Dewi, Leonardus Broto Sugeng Kardono & Arry Yanuar. 2017. Docking sulochrin and its derivative as α-glucosidase inhibitors of *Saccharomyces cerevisiae*. *Indonesian Journal of Chemistry* 17(1): 144-150. https://doi.org/10.22146/ijc.23568

Yamamoto, K., Miyake, H., Kusunoki, M. & Osaki, S. 2010. Crystal structures of isomaltase from *Saccharomyces cerevisiae* and in complex with its competitive inhibitor maltose. *FEBS Journal* 277(20): 4205-4214. https://doi.org/10.1111/j.1742-4658.2010.07810.x

Yaseen, R., Pushpalatha, H., Reddy, G.B., Ismael, A., Ahmed, A., Dheyaa, A., Ovais, S., Rathore, P., Samim, M., Akthar, M., Sharma, K., Shafi, S., Singh, S. & Javed, K. 2016. Design and synthesis of pyridazinone-substituted benzenesulphonylurea derivatives as anti-hyperglycaemic agents and inhibitors of aldose reductase – an enzyme embroiled in diabetic complications. *Journal of Enzyme Inhibition and Medicinal Chemistry* 31(6): 1415-1427. https://doi.org/10.3109/14756366.2016.1142986

Yuni Fatisa, Noval Herfindo, Fadila Aisyah, Hilwan Yuda Teruna, Jasril Jasril, Adel Zamri & Neni Frimayanti. 2025. Efficient synthesis using one-pot method and *in silico* analysis of pyridazinone derivatives as inhibitor for aldose reductase enzymes. *Trends in Sciences* 22(4): 9396. https://doi.org/10.48048/tis.2025.9396

Zheng, L., Meng, J., Jiang, K., Lan, H., Wang, Z., Lin, M., Li, W., Guo, H., Wei, Y. & Mu, Y. 2022. Improving protein – Ligand docking and screening accuracies by incorporating a scoring function. *Briefings in Bioinformatics* 23(3): bbac051. https://doi.org/https://doi.org/10.1093/bib/bbac051

*Corresponding author; email: jasril.k@lecturer.unri.ac.id